AGU ADVANCING EARTH AND SPACE SCIENCE

Earth and Space Science

RESEARCH ARTICLE
10.1029/2020EA001507

Reducing Systematic Biases Over the Indian Region in CFS V2 by Dynamical Downscaling

K. B. R. R. Hari Prasad[1], Dandi A. Ramu[2], Suryachandra A. Rao[2], Saji N. Hameed[3], Dhrubajyoti Samanta[4], and Ankur Srivastava[2]

[1]National Centre for Medium Range Weather Forecast (NCMRWF), Noida, India, [2]Indian Institute of Tropical Meteorology, Pune, India, [3]The University of AIZU, Aizu-Wakamatsu, Japan, [4]Asian School of the Environment, Nanyang Technological University (NTU), Singapore

Key Points:

- The seasonal mean dry bias is significantly reduced over the Indian sub-continent in WRFOML compared to the CFSv2-T126 and WRFCTL
- Mean annual cycle, standard deviation, and skill of rainfall over India are improved in WRFOML in comparison with CFSv2-T126 and WRFCTL
- Category-wise distributions of rainfall (particularly heavy rainfall >40 mm) are remarkably improved in the WRFOML than the CFSV2-T126 and WRF-CTL

Correspondence to:
S. A. Rao,
surya@tropmet.res.in

Citation:
Hari Prasad, K. B. R. R., Ramu, D. A., Rao, S. A., Hameed, S. N., Samanta, D., & Srivastava, A. (2021). Reducing systematic biases over the Indian region in CFS V2 by dynamical downscaling. *Earth and Space Science*, *8*, e2020EA001507. https://doi.org/10.1029/2020EA001507

Received 7 OCT 2020
Accepted 27 MAY 2021

Abstract The usefulness of dynamical downscaling of seasonal reforecasts of Indian Monsoon is explored to address the seasonal mean biases in the reforecasts. Almost all the current generation global coupled models, including the Climate Forecast System version 2 (CFSv2, T126 ~110 km), exhibit systematic mean dry bias over the central Indian region during the summer monsoon season. Cold sea surface temperature (SST) biases in the Indian Ocean and a weak monsoon circulation due to a colder tropospheric temperature contribute to this dry bias. Such systematic biases restrict the use of skillful forecasts from these models in climate applications (such as agriculture or hydrology). Dynamical downscaling of seasonal forecasts (~110 km resolution) using the Weather Research and Forecasting (WRF) model coupled to a simple ocean mixed layer model (OML; WRFOML) at 38 km resolution significantly reduces the majority of the systematic biases reported earlier. The seasonal mean dry bias reduces to 16% in WRFOML as compared to 44% (33%) in the CFSv2-T126 (WRFCTL) over the Indian land region. Warmer SSTs in the Indian Ocean and a more robust monsoon circulation emanating from a realistic simulation of the tropospheric temperature reduced the systematic biases in WRFOML compared to CFSv2-T126 and WRFCTL. Additionally, category-wise rainfall distributions are also improved drastically in the downscaled simulations (WRFOML). Downscaled reforecasts with reduced systematic biases have better suitability for climate applications.

Plain Language Summary Global modeling systems across the world suffer from different systematic biases and they have a coarse resolution which limits their usefulness for applications. An attempt is made to dynamically downscale forecasts from global models using regional models at a finer resolution. Such an approach results in improved simulation of rainfall over the Indian land region, hence making them useful for applications such as agriculture and hydrology.

1. Introduction

Southwest monsoon, from June to September (JJAS), is the primary rainy season for the Indian subcontinent, which contributes ~78% of India's total annual rainfall (e.g., Rajeevan et al., 2013). Variations in Indian summer monsoon rainfall (ISMR) on different time scales significantly impact agriculture, potable water, energy sector, food production, and gross domestic product (Gadgil & Gadgil, 2006), and the livelihood of millions of people living in the country. Thus, prediction of ISMR variability using global and regional models at a long lead time (i.e., 3–4 months in advance) is of great socio-economic importance. Toward achieving this goal, concerted efforts were undertaken by the monsoon community over the last decade to develop dynamical models and to improve the prediction skill of ISMR with dynamical models. These efforts were the outcome of the Indian Monsoon Mission (MM) Program (Rao et al., 2019). The high-resolution Climate Forecast System version 2 (CFSv2) was set up at the Indian Institute of Tropical Meteorology to provide experimental forecasts of the ISMR since 2009 and is now operational in India Meteorological Department since 2017. The model has a reasonably high skill in predicting ISMR (Ramu et al., 2016; Rao et al., 2019) and the homogenous regions of the Indian sub-continent (Ramu et al., 2017) at the longer lead time (i.e., February Initial conditions). Based on the MM phase I's success, the MM phase II was launched with an emphasis on developing applications based on the skillful seasonal forecasts of ISMR. Seasonal forecasting is built on the realms of ensemble forecasting and noise reduction techniques. Various techniques are used to filter out the climatic "noise" from the seasonal forecasts. Time and spatial mean

effectively suppress the spatial and temporal variability in the forecasts arising out of the high-frequency weather events. Therefore the country averaged seasonal forecasts, such as ISMR, exhibit robust skill scores. However, many global models suffer from significant spatial mean biases and are unable to deliver useful information at the regional or local spatial scales. For example, the seasonal rainfall forecast at different stages of growth and development of the crop is essential. The meteorological inputs as seasonal means from coupled general circulation models (CGCMs) are not enough for the proper planning of the entire crop season (Capa-Morocho et al., 2016). Seasonal forecasts of all India averaged rainfall limit its applicability to agriculture, hydrology, energy, and other sectors (Manzanas et al., 2018; Ramu et al., 2017; Sabeerali et al., 2013; S. K. Saha et al., 2016). Many crop or hydrology models are configured at smaller regional scales and hence can be significantly affected by the biases of the dynamical models, and country averaged information has little value. Generally, many global coupled models show wet bias in seasonal mean precipitation over oceans and dry bias over land regions (e.g., George et al., 2016; B. B. Goswami et al., 2014; Pillai et al., 2018; Ramu et al., 2016; S. K. Saha et al., 2013). Hence, it is imperative to develop techniques to reduce the systematic biases of CGCMs and provide information at smaller spatial scales. Numerous attempts have been made in the past to demonstrate the capability of regional climate models (RCMs) to simulate the Indian summer monsoon (ISM) and its mean features (Bhaskar Rao et al., 2004; Bhaskaran et al., 1996; Dobler & Ahrens, 2010; Hari Prasad et al., 2011; Jacob & Podzun, 1997; Lee & Suh, 2000; Lucas-Picher et al., 2011; Mukhopadhyay et al., 2010; Raju, Parekh, & Gnanaseelan, 2014; Raju, Parekh, Chowdary, et al., 2014; Saeed et al., 2012; Srinivas et al., 2012; Vernekar & Ji, 1999). Recently, several studies (X. Chen et al., 2018; Misra et al., 2018; Wu et al. 2018) have assessed the monsoon intraseasonal oscillation using regional models and mentioned that the explicit convection could improve the ISM simulation. Most recently, Konduru and Takahashi (2020) studied the effects of convection and horizontal resolution on the rainfall characteristics of ISM. They suggested that cumulus parameterization plays a vital role in initiating the more frequent, widespread precipitation over the Indian land region.

Dynamical downscaling with RCMs can transfer global predictions from CGCMs to regional or local spatial scales (Manzanas et al., 2018). These RCMs are forced by initial and lateral boundary conditions from General Circulation Models (GCMs). They can better represent the mesoscale circulations, topography, land-use, and land cover, and thereby these models improve the regional climatic variability and extremes compared to the coarse resolution GCMs (Dash et al., 2014; Di Luca et al., 2012; Giorgi & Gutowski, 2015; Jacob & Podzun, 1997; Juang et al., 1997; Maharana & Dimri, 2016; Ratnam et al., 2013; Samanta et al., 2018; Stéfanon et al., 2014; Vellore et al., 2014; Vernekar & Ji, 1999; Xue et al., 2014). Torma et al. (2015) also stated that the RCMs could improve precipitation patterns compared to those obtained from driving GCMs. More recently, Devanand et al. (2018) demonstrated that the dry bias of ISMR over the Ganga basin could be reduced by the dynamical downscaling of CFSv2-T126 free run by using Weather Research and Forecasting (WRF) model coupled to land surface models, and hence their usability is needed to be explored from a forecasting perspective. They attributed these improvements to the enhanced moisture transport from the Western and Upper Indian Ocean to Ganga Basin, which leads to improved precipitation recycling over the Ganga basin. Similarly, Samanta et al. (2018) simulated the ISM using a regional coupled model (WRF coupled to simple ocean model) by taking the initial and boundary conditions from CFSv2-T126 free run; and found that there is a significant reduction in the seasonal dry bias over central India because of a warm coastal Bay of Bengal sea surface temperature (SST) front. In short, the regional dynamical models can reduce some of the systematic mean biases of the CGCMs, which might be useful for hydrological applications (Devanand et al., 2018; Samanta et al., 2018). Ramu et al. (2016) have shown that the rainfall biases reduce over the central Indian region, and ISMR skill also improves in high-resolution CGCM compared to lower resolution model, due to better representation of teleconnection patterns among ISMR, El Nino and Southern Oscillation, and Indian Ocean mode. However, running a CGCM at a resolution higher than that in Ramu et al. (2016, ~38 km) is computationally very expensive. Therefore, employing a regional model to downscale the seasonal forecasts from CFSv2 seems to be an exciting alternative and forms the basis of the present study.

This study mainly aims to verify whether the dynamical downscaling with a coupled and uncoupled regional model can provide any value addition to these forecasts and if so, to investigate those improvements in reducing the seasonal mean rainfall dry biases over the central Indian region through dynamical downscaling of seasonal forecasts of CFSv2-T126. The structure of this article is as follows. Section 2 provides a brief

description of the models, data, and methodology used in this study. Section 3 presents the model simulated mean ISM features. Section 4 describes the simulation of extreme rainfall over the Indian region. The vertical structures of dynamic and thermodynamic components over different regions and climatological mean evolution of Tropospheric Temperature (TT), Moist Static Energy (MSE), and specific humidity averaged over 70°–90°E are described in Section 5. The final section summarizes the present study.

2. Models, Data, and Methodology

2.1. Model Description

The CFSv2-T126 (∼110 km) is a state-of-the-art coupled ocean-land-atmosphere-sea ice model developed by the National Center for Environment Prediction (NCEP: S. Saha et al., 2014) currently used by the India Meteorological Department (IMD) for seasonal prediction of monsoon (Pai et al., 2017). It may be noted that IMD operationally runs this model at a very high resolution (CFSv2-T382, ∼38 km, Pai et al., 2017; Ramu et al., 2016). The NCEP Global Forecast System is the atmospheric component of CFSv2 with a spectral triangular truncation of 126 waves (T126) in the horizontal (∼110 km) and 64 sigma-pressure hybrid levels in the vertical. CFSv2-T126 uses simplified Arakawa-Schubert convection with cumulus momentum mixing, orographic gravity wave drag. It is coupled with a four-layer Noah land surface model (Ek et al., 2003) and a two-layer sea ice model. The Oceanic component of CFSv2-T126 is the Modular Ocean Model version 4p0d (MOM4; Griffies et al., 2004) from the Geophysical Fluid Dynamics Laboratory. It has a zonal resolution of 0.5° and a meridional resolution of 0.25° within 10°S and 10°N and it becomes gradually coarser through the tropics up to 0.5°, and it uses 40 levels in the vertical. The atmosphere and ocean models are coupled with no flux adjustment. In this study, CFSv2-T126 hindcast runs are made with February initial conditions and integrated for nine months during 1982–2017 on the Pratyush High-Performance Computing system. It is an ensemble of 10 members initialized at 00 and 12 UTC every fifth day of February.

The WRF version 3.4 regional mesoscale model developed by the National Center for Atmospheric Research, USA, is used in this study for the dynamical downscaling of CFSv2-T126 seasonal hindcasts. WRF is a fully compressible, mass conservative finite difference model and uses Euler non-hydrostatic equations, Arakawa-C grid staggering for horizontal discretization, and terrain-following hydrostatic pressure vertical coordinate (Skamarock et al., 2008). The physical parameterizations used in WRF are Rapid Radiative Transfer Model for GCMs for long wave and short wave radiation (Iacono et al., 2008), Unified Noah land-surface model (F. Chen et al., 2001) for land surface processes, WRF double moment class-5 for microphysics (Lim & Hong, 2010), and Mellor-Yamada-Janjic TKE closure (Janjic, 1994; Mellor & Yamada, 1982) for boundary layer turbulence parameterization. Simulation of the Indian monsoon is known to be sensitive to the representation of cloud physics in the climate models (Mukhopadhyay et al., 2010). Based on previous studies (e.g., Mukhopadhyay et al., 2010; Srinivas et al., 2013), Betts-Miller-Janjic cumulus parameterization scheme (Betts & Miller, 1986; Janjic, 2000) given better performance in simulating the ISM climatological features. Physics options for the present study are used based on the previous study by Samanta et al. (2018). In this study, the WRF model is configured with a single domain over 37°S–44°N and 31°E–135°E with a horizontal resolution of 38 km, and 38 vertical levels are extending from surface to 50 hPa, which is considered in line with the model resolution used by the Coordinated Regional Downscaling Experiment regional climate simulations and this spatial resolution is adequate to resolve the hydrology related processes for seasonal scale simulations and enough to capture the appropriate synoptic-scale phenomena governing the climate over ISM region (e.g., Dobler & Ahrens, 2010; Raju et al., 2015).To understand the role of air-sea interaction on the mean monsoon features in the WRF, we have conducted two experiments: (i) WRF is forced by daily observed Optimum Interpolated SST as a lower boundary condition (WRFCTL), and (ii) WRF is coupled to the ocean mixed layer model (WRFOML). OML is a simple one-dimensional linearized Boussinesq model (Davis et al., 2008; Pollard et al., 1972). It requires the specification of the initial depth of the mixed layer and deep layer temperature lapse rate, it gets the heat fluxes and wind stress from WRF and computes SST, and it serves as a lower boundary condition for the atmospheric model. Since it is a one-dimensional model, there is no direct exchange of properties between the model grid points (i.e., advection); this may lead to slight errors in the estimation of SST. WRFOML is initialized using the observed climatological mixed layer depth (MLD) for February-September, and SST is updated at every model time step. The WRF model is forced with the initial and lateral boundary conditions from the ensemble means

of CFSv2-T126 hindcast runs. Ten gridpoints at the lateral boundaries are used to nudge the regional model fields toward the global model, and we have not used any spectral nudging. Both the experiments were initialized at 00UTC on 26th February of each year and integrated upto 1st October during 1982–2017. The ensemble mean of these 10 members is used as the lateral boundary conditions for WRFOML.

2.2. Data and Methodology

To validate the model simulated SST, we have used monthly observed Optimum Interpolated SST (OISST, Reynolds et al., 2002; https://psl.noaa.gov/data/gridded/data.noaa.oisst.v2.html) with a spatial resolution of 1.0° × 1.0° during 1982–2017. For rainfall validation, we have obtained monthly rainfall from Global Precipitation Climatology Project (GPCP, Adler et al., 2003; https://rda.ucar.edu/datasets/ds728.3/) with a spatial resolution of 2.5° × 2.5° and daily Tropical Rainfall Measuring Mission (TRMM) estimated monthly precipitation available from https://disc.gsfc.nasa.gov/datasets/TRMM_3B42_Daily_7/summary (3B43V7, Huffman et al., 2007), and gridded rainfall data from India Meteorological Department (IMD; Rajeevan et al., 2006; http://www.imdpune.gov.in/Clim_Pred_LRF_New/Grided_Data_Download.html) over India with 1° × 1° resolution. The model generated monthly large-scale atmospheric fields are compared with European Center for Medium-Range Weather Forecast (ECMWF) interim reanalysis (ERA-interim) monthly data products such as winds, air temperature, specific humidity at different levels, and sea level pressure (Dee et al., 2011; https://apps.ecmwf.int/datasets/data/interim-full-daily/levtype=pl/) for the same period. The Ocean mixed Layer model is initialized using the mixed layer depth obtained from https://www.metoffice.gov.uk/hadobs/en4/, which is based on observed Ocean temperature and salinity profiles.

Further, to understand the thermo-dynamical response, moist static energy (MSE, which is a measure of vertical instability; Kim et al., 2014) is estimated using the following equation:

$$MSE = C_p T + gz + L_v q \tag{1}$$

where C_p is the specific heat at constant pressure, T is temperature, g is gravity, z is geopotential height, L_v is the latent heat of vaporization, and q is specific humidity.

Moisture availability plays a significant role in monsoon initiation and sustenance (Pradhan et al., 2017). Hence, we have calculated vertically integrated moisture transport (VIMF) using the following expression (Fasullo & Webster, 2003):

$$VIMF = \int_{1000}^{300} qUdp \tag{2}$$

where q is the specific humidity, and U is the wind vector. Vertical integration was performed from 1000 to 300 hPa. Monsoon season can be differentiated into non-rainy and rainy days based on the amount of rain received. Rainy days are further classified into different rainfall intensity categories, viz. light rain (1–10 mm), moderate rain (10–40 mm), and heavy rain (>40 mm) (Mukhopadhyay et al., 2010). The frequencies of rainfall intensities are calculated based on Dai (2006), which is given as follows

$$\text{Frequency} = \left(\frac{\text{Number of rainy days in that particular rainfall intensity category}}{\text{Total number of rainy days}} \right) * 100 \tag{3}$$

Apart from this, to assess the model's ability, we have used different standard statistical metrics such as mean, standard deviation (SD), root mean square error (RMSE), mean absolute error (MAE) and bias (model-observation), and skill as the anomaly correlation coefficient between observation and model. Model products are interpolated by using the bilinear interpolation method according to the resolution of the observations. All analysis is carried out for JJAS season only.

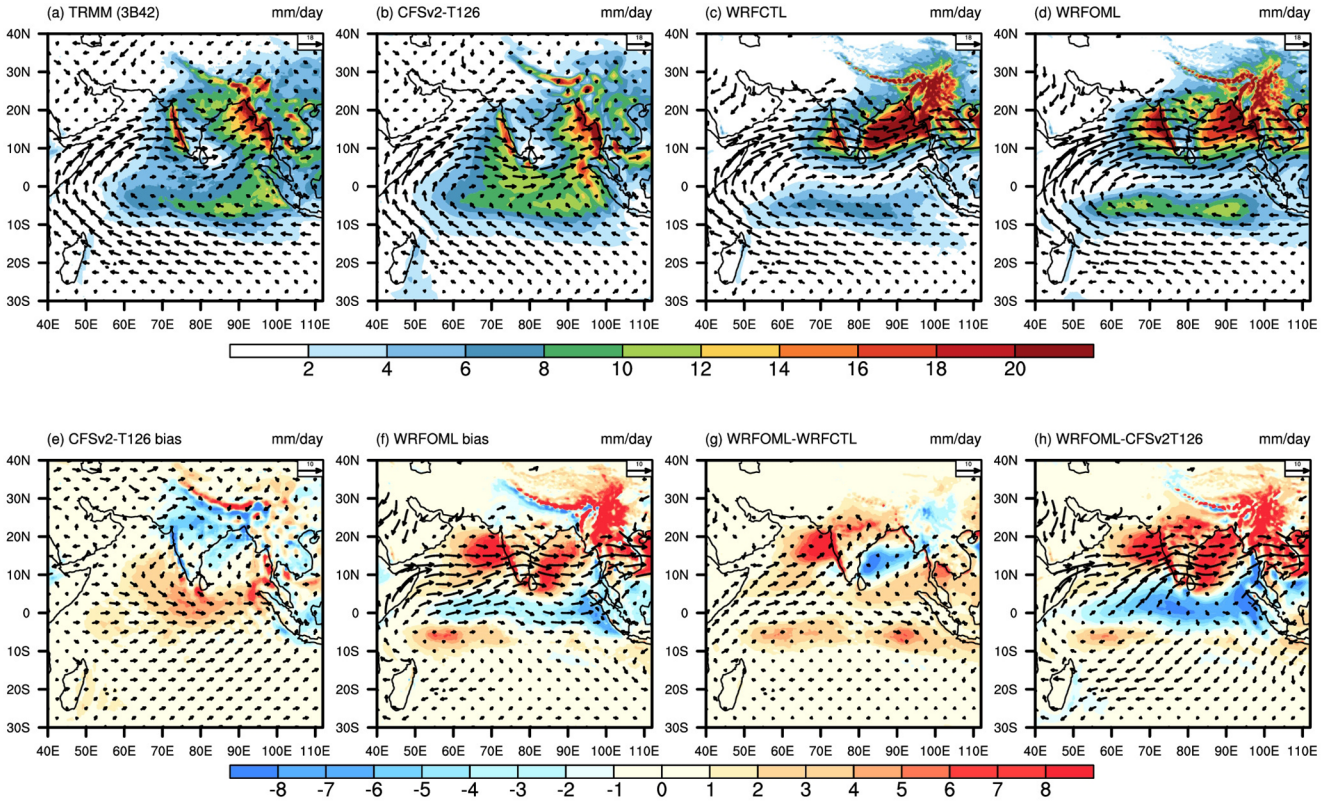

Figure 1. Spatial distribution of mean precipitation (mm/day, shaded) and winds at 850 hPa (m/s, vectors) from (a) observation, (b) CFSv2-T126, (c) WRFCTL, and (d) WRFOML. The biases of the models (e) CFSv2-T126 and (f) WRFOML from the observation and (g) difference between WRFOML and WRFCTL, and (h) difference between WRFOML and CFSv2-T126.

3. Results and Discussion

The impact of dynamical downscaling of CFSv2-T126 reforecast runs on the ISM mean feature and its prediction skill with a coupled and uncoupled WRF model is presented here. A brief description of the large scale seasonal mean features and their systematic mean biases (bias; model-observations) over ISM region for different atmospheric and oceanic parameters like lower and upper tropospheric circulations, precipitation, SST, sea level pressure (SLP), Tropospheric Temperature (TT), vertically Integrated (950-150 hPa) moist static energy (MSE), vertically integrated moisture transport (surface-300 hPa) and Hadley circulation over Indian longitudes (averaged 70°–90°E) are given in the subsequent sections, which reveals the capability of the models to simulate the mean monsoon features.

3.1. Simulation of Important Climatological Features of ISM

In this section, the large-scale mean features of the Indian summer monsoon are described. Figure 1 elucidates the spatial distribution of climatological JJAS mean precipitation and low-level circulation patterns at 850 hPa from the observations and model simulations and their mean biases. It is noted that major convective centers are seen over the eastern Arabian Sea (AS), Bay of Bengal (BoB), central, western coast, and north-east Indian regions in the observation (TRMM) (Figure 1a). CFSv2-T126 is unable to reproduce mean seasonal rainfall over the central Indian region compared to the observation (Figure 1b), whereas WRFOML (Figure 1d) could simulate the seasonal mean rainfall over the central Indian region and the equatorial Indian Ocean compared to CFSv2-T126 and WRFCTL. Even though CFSv2-T126 well represents the convective centers over the ocean, a dry mean bias still persists same as in many coupled model Intercomparison Project Phase 5 and U.S. nation multimodel ensemble models over the central Indian region (George et al., 2016; B. B. Goswami et al., 2014; Pokhrel et al., 2013; Pillai et al., 2018; Ramu et al., 2016; Sabeerali et al., 2013; S. Saha et al., 2014; S. K. Saha et al., 2016). The dry bias over India is primarily attributed to the cold SST bias

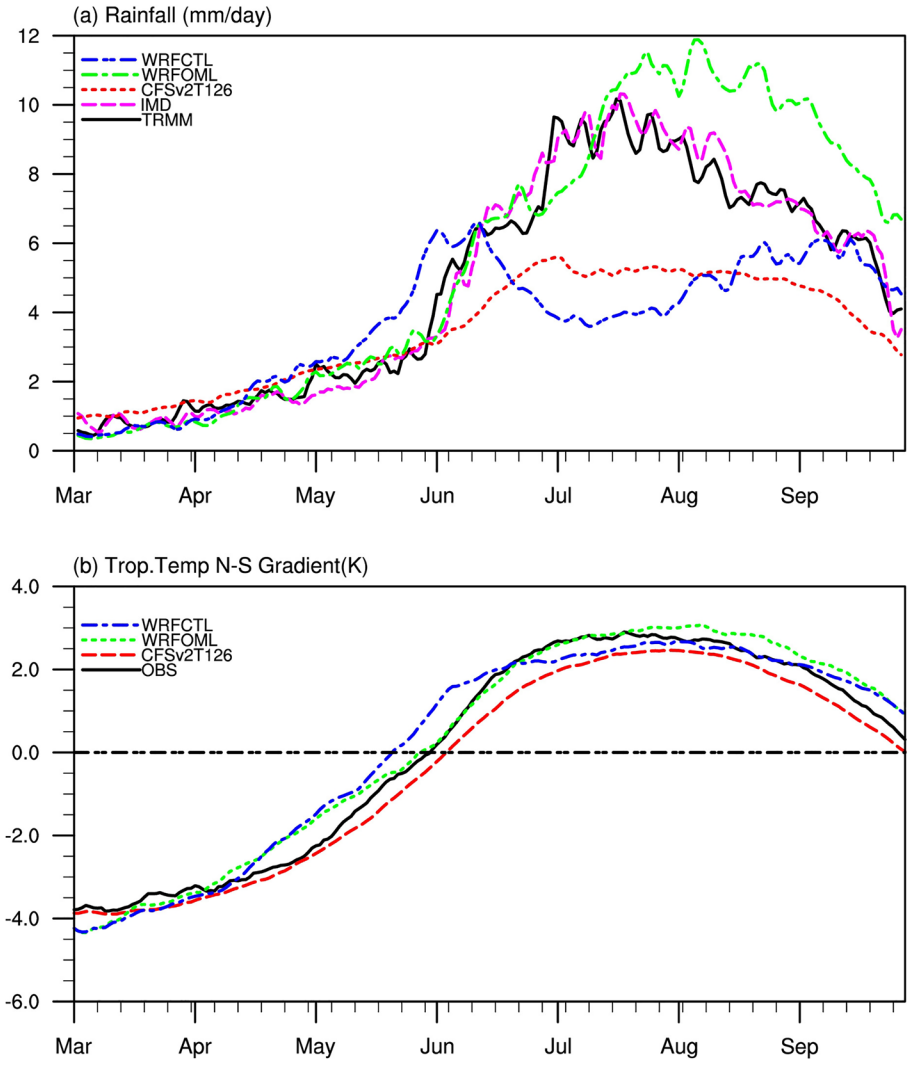

Figure 2. The climatological annual cycle of (a) area-averaged rainfall over Indian landmass and (b) tropospheric temperature gradient. The black (TRMM) and pink (IMD) lines represent the observation, the red line represents CFSv2-T126, the green line represents WRFOML, and the blue line represents WRFCTL.

in the Indian Ocean (Figure 2b) and the presence of an anomalous anti-cyclone over the central Indian region, thereby inhibiting the propagation of rain-bearing monsoon low-pressure systems over India (George et al., 2016; Srivastava et al., 2017). The dry bias over the central Indian region is significantly reduced in WRFOML compared to CFSv2-T126 and WRFCTL, which is consistent with the recent study by Samanta et al. (2018). In the CFSv2-T126 simulation, there is a strong wet bias over the equatorial and central Indian ocean, whereas there is a dry bias in the downscaled simulations (Figures 1e and 1f). It is noticed that WRFCTL has a strong wet bias over AS and BoB, and which is slightly reduced in WRFOML. It is important to note that both WRFCTL and WRFOML overestimated the mean precipitation along the mountains (the Western Ghats and Himalayan region) compared to CFSv2-T126 (Figures 1c and 1d). A recent study has shown that orographic precipitation is improved in higher horizontal resolution (CFSv2-T382) than in the coarse resolution models (CFSv2-T126) (Konduru Takahashi, 2020; Ramu et al., 2016). An important dynamical feature of ISM is the formation of the strong cross-equatorial jet at lower levels (850 hPa), which is also known as the Findlater jet (Joseph & Raman, 1966; Findlater, 1969). This low-level jet (LLJ) is an essential source of moisture for the Indian monsoon (Findlater, 1969; Swathi et al., 2020). All the model simulations are able to capture the mean LLJ reasonably well, but CFSv2-T126 is simulated as a weak LLJ (Figures 1b–1d), which implies lesser moisture availability to the monsoon circulation. WRFOML shows a more

Table 1
Model Statistics of Indian Summer Monsoon Rainfall (ISMR) Averaged Over the Indian Land Region

Indian landmass	CFSv2-T126	WRFOML	WRFCTL	IMD
Mean	4.17	8.7	4.9	7.48
Standard deviation (SD)	0.36	0.59	0.9	0.64
Bias (model-observation)	−3.3	1.2	−2.5	
Mean absolute error	3.3	1.2	2.3	
RMSE	3.35	1.35	2.6	
Skill	**0.50**	**0.54**	0.48	

Note. Values significant at 95% confidence level are highlighted in bold.

robust south-westerly mean flow over the Indian Ocean and the Indian landmass, whereas relatively weaker south-easterlies over the southern Indian Ocean compared to the CFSv2-T126. WRFOML simulated strong south-westerlies over the AS and equatorial Indian Ocean region (Figure 1g) compared to CFSv2-T126 and WRFCTL, which helps to transport more moisture to AS and Central Indian region and thereby reduces the dry bias in WRFOML. WRFCTL simulated strong south-westerlies, which transported more moisture to the BoB region than WRFOML, which causes strong wet bias in WRFCTL.

Area averaged seasonal rainfall evolution over the Indian land points from the observations (IMD & TRMM), CFSv2-T126, WRFCTL, and WRFOML are shown in Figure 2a. In observations, the rapid increase in rainfall is noticed in June 1st week (monsoon onset), and it peaks during July-August. It gradually declines in September (Figure 2a). CFSv2-T126 is unable to represent the sharp increase in the rainfall from June and a sharp decrease from September as in observations. It is noticed that in WRFCTL, rainfall started two weeks ahead of the observations and matches with observations in the first week of June and the last week of September. It has a significant dry bias over the Indian land region during the peak monsoon months (i.e., July and August). There is a considerable improvement in the simulated annual cycle, and it is more realistic in WRFOML compared to the other experiments. Both CFSv2-T126 and WRFCTL failed to simulate adequate rainfall in the peak monsoon months (i.e., July and August) compared to the WRFOML. The dry bias over the Indian land region in CFSv2-T126 may be attributed to the cold SST bias and weaker south-westerly flow over the Indian ocean. In the case of WRFCTL, dry bias over central India may be attributed to the lack of ocean coupling. It is noticed that in WRFOML, ISMR mean and SD are closer to the observations compared to CFSv2-T126 and WRFCTL (Table 1). The prediction skill of ISMR (correlation between observed rainfall anomalies averaged over Indian land region and re-forecasted anomalies) is slightly better in WRFOML compared to WRFCTL and CFSv2-T126 (Table 1). The mean onset date of the Indian summer monsoon is studied based on the TT gradient (B. N. Goswami & Xavier, 2005) from observation and model simulations The date when the TT gradient changes from negative to positive can be considered as the onset date of monsoon and when it changes the sign from positive to negative, it can be considered as the withdrawal of monsoon. From Figure 2b, it is noticed that the CFSv2-T126 simulated delayed onset and early withdrawal, which is consistent with the previous study by Pradhan et al. (2017), whereas WRFCTL simulated early onset compared to WRFOML. Overall, the WRFOML simulates a mean onset date of 28th May, which is close to the observation (30th May) and has a stronger TT gradient compared to the CFSv2-T126 and WRFCTL (Figure 2b).

4. Systematic Error in Simulated Rainfall Distribution and IAV of ISMR

To explore the spatio-temporal variability of rainfall superimposed on the JJAS seasonal mean, we have computed daily mean rainfall probability distribution functions (PDFs) from different ranges of rain rates over different regions, frequency of categorical rainfall, and Inter-annual variability (IAV) of rainfall over the Indian region from CFSv2-T126, WRFCTL, WRFOML, and the observation during the summer monsoon season.

4.1. PDF for Different Rain Rates

In this section, we examine PDF of daily rainfall at four major precipitation areas: Central India (CI; 70°E–90°E; 18°N–26°N), BoB (86°E–94°E; 14°N–22°N), AS (68°E–74°E; 12°N–21°N), and Equatorial Indian Ocean (EIO; 75°E–90°E; 10°S–0°) for three rain-rate categories (lighter: <10 mm day^{-1}, moderate:10–40 mm day^{-1} and heavy: >40 mm day^{-1}) based on Abhik et al., (2013) are shown in Figure 3. Abhik et al. (2013) have reported that a better simulation of the frequency distribution of rain rates translates to a realistic simulation of the mean state of monsoon. In CFSv2-T126, the contribution of the light rain category to the total rain is significantly overestimated, and the simulated PDF shows a large difference compared to the observed PDF in these areas, which is corroborated with the previous study by Krishna et al. (2019).

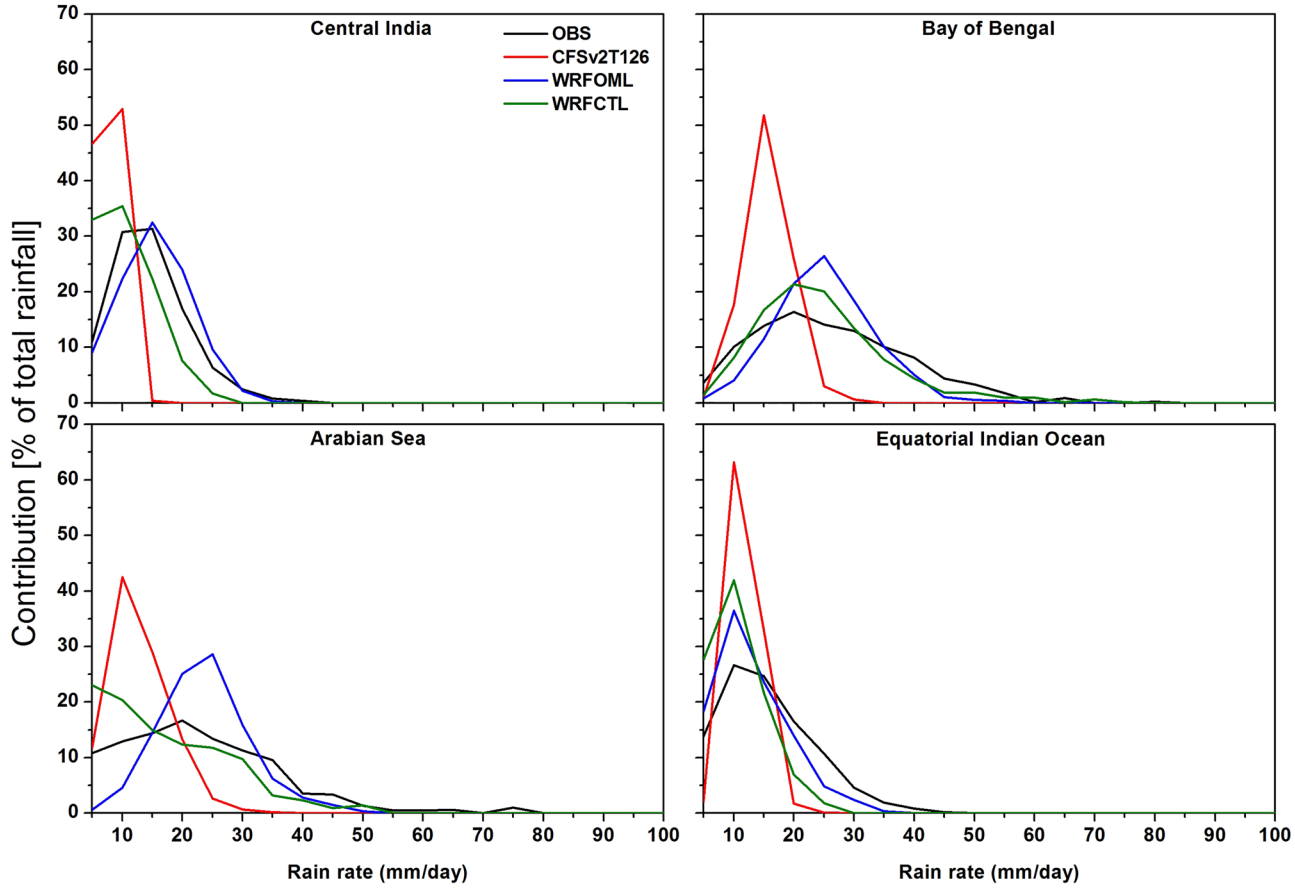

Figure 3. Comparison of model-simulated probability distribution functions for different rain rate categories, based on daily JJAS precipitation over (a) central India (18°N−28°N; 70°E−90°E), (b) Bay of Bengal (14°N−22°N; 86°E−94°E), (c) Arabian Sea (12°N−21°N; 68°E−74°E), and (d) equatorial Indian Ocean (10°S–0°; 75°E−90°E) with observation.

But, CFSv2-T126 significantly underestimates the contribution from moderate and heavy rain categories to the total rain over these four regions compared to the observations. Both WRF experiments are well captured the different rainfall categories over these regions compared to CFSv2-T126. The WRFOML is well simulated different rainfall categories over the CI and EIO compared to the WRFCTL. Thus, WRFOML is able to reproduce all rainfall categories over CI compared to WRFCTL and CFSv2-T126, which reduces the mean dry biases in that region (Figure 1f).

4.2. Spatial Distribution of Frequency of the Rainfall

Spatial distribution of rainfall characteristics in terms of frequency of no rain days, rainfall intensity in different rain-rate categories such as light, moderate and heavy for the season as a whole from the observations and model simulations are shown in Figure 4. The classification of rainfall intensity in different categories and the calculation of frequency of the rainfall are described based on an earlier study by Mukhopadhyay et al. (2010) (more details are given in Section 2.2). Observation shows that the frequency of no rain days (50%–70%) is more over North West (NW) India and is significantly less over the monsoon core region and North East India. It is observed that the frequency of moderate rain category is high over the monsoon core region and NE India. Both WRF model simulations capture the no rain days over Indian landmass reasonably well, but with significant underestimation in CFSv2-T126 (Figures 4a–4d). WRFOML and WRFCTL could capture the light rain category better with slight overestimation over southern peninsular India (Figures 4e–4h), whereas CFSv2-T126 overestimates this rain category almost over entire India and the same is noted in PDF (Figure 3) as well. CFSv2-T126 significantly underestimates the moderate rain-rate category over most parts of the country (Figure 4j). WRFCTL well represented the moderate rain

10.1029/2020EA001507

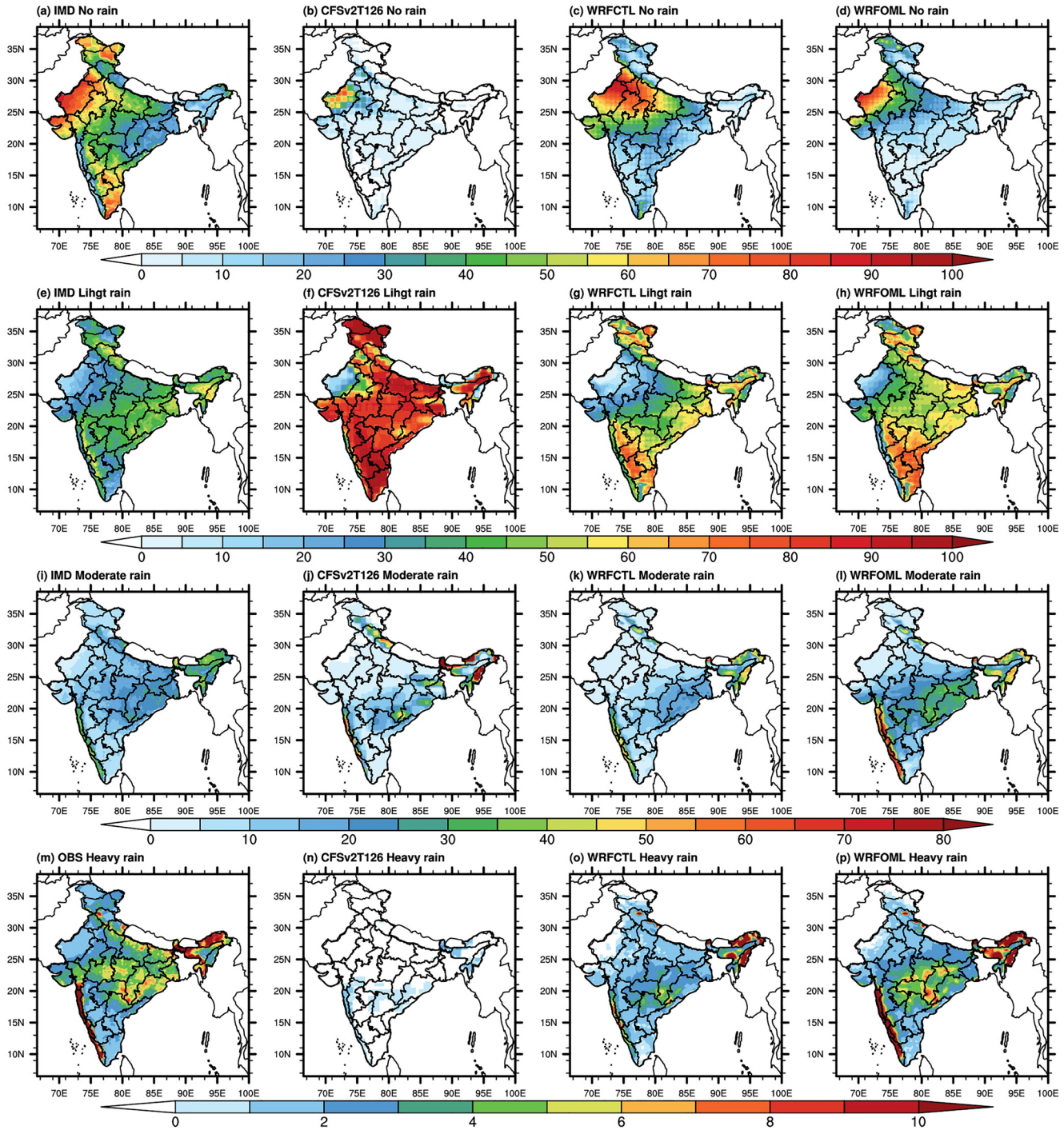

Figure 4. JJAS mean spatial frequency distribution of different rain rate categories: (a–d) no rainy days, (e–h) light rain, (i–l) moderate rain, and (m–p) heavy rain. The first column is from observation, second, third, and fourth columns represent CFSv2-T126, WRFCTL, and WRFOML, respectively.

categories compared to CFSv2-T126 and WRFOML (Figure 4l). Among these rain categories, the spatial pattern of the heavy rain category is well represented by the WRFOML than CFSv2-T126 and WRFCTL (Figure 4p). Additionally, we have examined the average number of rainy days (≥2.5 mm day^{-1}) over Indian landmass and five homogeneous regions of India viz. NWI (North-West India), NEI (North-East India), CNEI (Central North East India), WCI (West Central India), and SPI (Southern Peninsular India) (Ramu et al., 2017) from the model simulations and the observation. Information on the number of rainy days

Table 2
The Statistics of Rainy Days (≥2.5 mm/day) for Observations (IMD) and Models (CFSv2-T126, WRFOML, and WRFCTL) for the Period of 1982–2017

	Skill (ACC)			Mean				SD			
Region	CFSv2-T126	WRFOML	WRFCTL	OBS	CFSv2-T126	WRFOML	WRFCTL	OBS	CFSv2-T126	WRFOML	WRFCTL
India	**0.39**	**0.51**	0.22	46	66	62	56	3.8	5.2	4.2	6.9
Northeast India (NEI)	0.27	0.19	0.0	76	116	97	94	6.6	1.7	3.9	6.8
West-central India (WCI)	**0.28**	**0.44**	0.21	55	67	61	59	5.9	10.8	7.9	11
Northwest India (NWI)	0.1	**0.32**	0.0	27	9	30	12	6.2	3.2	6.4	4
Central North East India (CNEI)	0.16	0.23	0.19	55	71	68	55	5.5	9.6	6.9	10.8
South Peninsular India (SPI)	**0.3**	0.16	0.2	45	76	68	79	5.2	6.6	5.1	11.4

Note. Values significant at 90% and 95% confidence level are highlighted in bold.

during the monsoon season is crucial from an agricultural and hydrological perspective. Table 2 summarizes the statistics of rainy days from observation and the model simulations during the monsoon season for the period 1982–2017. Though all the model simulations have over-estimated the number of rainy days over Indian land points, WRFOML and WRFCTL could represent the number of rainy days better than CFSv2-T126. Overall, the skill of the model in simulating the number of rainy days is better in downscaled WRFOML simulation (WRFOML: 0.51, CFSv2-T126: 0.39, and WRFCTL: 0.22). Skill improvements are also noticeable over WCI, NWI, and CEI.

4.3. Inter-Annual Variability of ISMR

The year-to-year variations of the model simulated Indian summer monsoon rainfall (ISMR) and India Meteorological Department (IMD) gridded rainfall data from 1982 to 2017 are given in Figure 5. The correlation coefficient between the IMD (GPCP) and simulated ISMR are 0.50 (0.4), 0.50 (0.4), and 0.54 (0.55) for CFSv2-T126, WRFCTL and WRFOML, respectively. Among the 36 years of hindcast period, CFSv2-T126 is failed to capture the correct phase of ISMR in nine years (1985, 1989, 1990, 1993, 1997, 2011, 2013, 2014, and 2015), WRFCTL failed to capture the correct phase in nine years (1982, 1984, 1985, 1990, 1993, 1997, 2002, 2013, and 2015), and WRFOML also failed to capture the correct phase of ISMR in seven years (1982, 1984, 1990, 1993, 1999, 2005, and 2013). CFSv2-T126 tends to underestimate the SD of ISMR (0.36 mm day^{-1}) compared to the observations. Interestingly, WRFOML better simulated the ISMR with an SD of 0.59 mm day^{-1} which is closer to the observations (IMD: 0.64 mm day^{-1} and GPCP: 0.62 mm day^{-1}). A 16% reduction in the dry bias over the Indian region is noted in WRFOML compared to CFSv2-T126 (44%) and WRFCTL (33%). Similarly, ISMR biases, RMSE, MAE are improved in WRFOML compared to CFSv2-T126 and WRFCTL (Table 1).

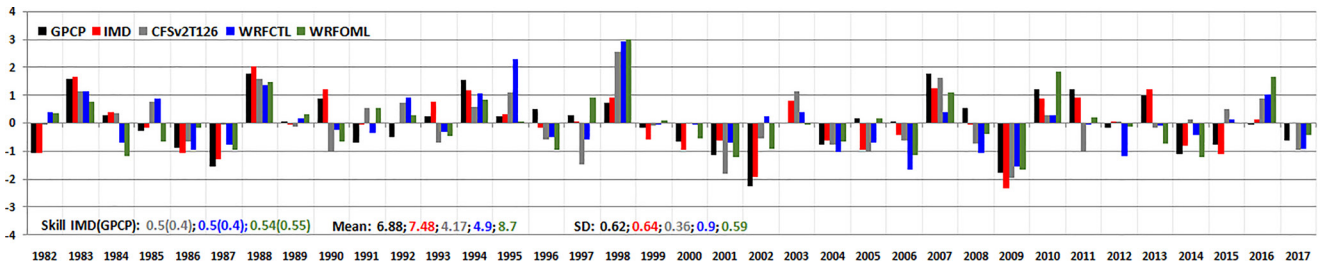

Figure 5. Inter-annual variability of ISMR normalized anomalies for CFSv2-T126, WRFCTL, and WRFOML simulations along with observations. Model skill, mean, and standard deviation (SD) are given at the bottom of the figure.

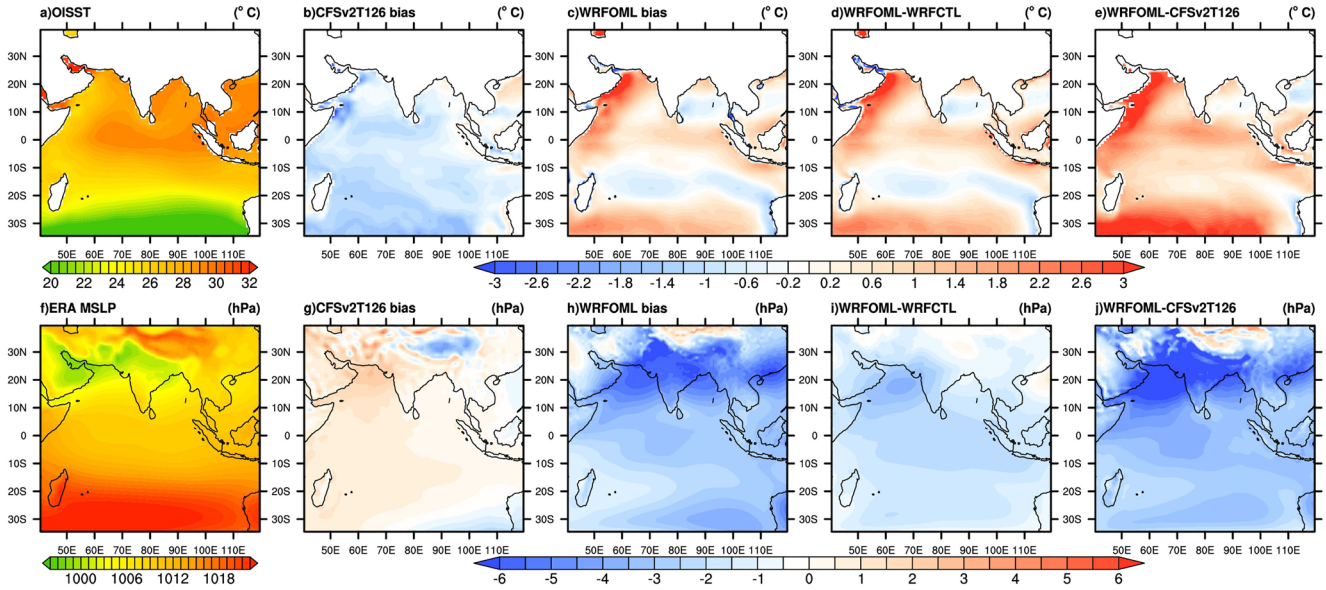

Figure 6. Spatial distribution of (a) mean SST (°C) from observation, the biases from (b) CFSv2-T126, and (c) WRFOML and (d) difference between WRFOML and WRFCTL, (e) difference between WRFOML and CFSv2-T126. The lower panel (f–j) is the same as the upper panel but for MSLP (hPa).

It is also interesting to note that the mean and variability of rainy days have improved over all the homogenous regions. The improvement in simulating the length of rainy days by WRFOML can be attributed to the sufficient water vapor availability in the atmosphere compared to CFSv2-T126 and WRFCTL.

Figure 6 shows the spatial distributions of JJAS mean SST and SLP from observation and the biases in the model simulations. It is found that the CFSv2-T126 model has a strong cold bias over the entire Indian ocean (Figure 6b), WRFOML has a warm SST bias over the west coast of AS, head Bay of Bengal (BoB), equatorial Indian Ocean, and south of 20°S, it may be attributed to the lack of ocean advection in WRFOML (Umakanth et al., 2016) (Figure 6c). SST differences between WRFOML and WRFCTL (which is forced by OISST) (Figure 6d) show that the WRFOML has warm bias over most parts of the Indian ocean, which enhanced the latent heat flux and the transport of moisture to the Indian land region. Even though the WRFOML (Figure 6h) under predicts the SLP, it could represent the location of surface heat low over northwest India and the position of the monsoon trough reasonably well compared to CFSv2-T126 (Figure 6g).

Previous studies have reported that upper tropospheric temperature (TT) over the Asian summer monsoon region has a dominant role in maintaining the monsoon circulation (B. N. Goswami & Xavier, 2005; Xavier et al., 2007). The TT is simulated well in WRFOML than the other experiments. CFSv2-T126 shows a strong cold bias over the entire ISM region (Figure 7b). WRFCTL is also shown significant cold bias over the ISM region (Figure not shown). WRFOML simulated a warmer TT compared to WRFCTL (Figure 7d), which indicates more convectively unstable and enhanced mean monsoon flow in WRFOML. This cold tropospheric temperature causes a weaker monsoon circulation in CFSv2-T126 as well as in WRFCTL simulations. The cold TT bias is significantly reduced, and the strong north-south temperature gradient is simulated well in WRFOML. Additionally, to understand the thermo-dynamical response of monsoon, the vertically integrated (from 950 to 100 hPa) MSE, a measure of vertical instability, are also analyzed. Higher values of precipitable water lead to excess MSE at the lower troposphere, supporting unstable boundary layer, convective ascent, and excessive rainfall (Emanuel et al., 1994; Sabin et al., 2013). In the observation, the maximum MSE is located in the monsoon trough region (as this is the region of formation and propagation of low-pressure systems), while in CFSv2-T126, underestimation of MSE is noticed, corroborating with the conclusion of Samanta et al. (2018) that the inadequacy of CFSv2-T126 in capturing the low-pressure systems (Srivastava et al., 2017). WRFOML could capture JJAS mean MSE spatial pattern reasonably well with a slight overestimation compared to WRFCTL. The positive MSE bias in WRFOML compared to the CFSv2-T126 and WRFCTL indicates that the atmosphere is more convectively unstable, which supports large-scale ascent and precipitation (Figures 4g and 4h).

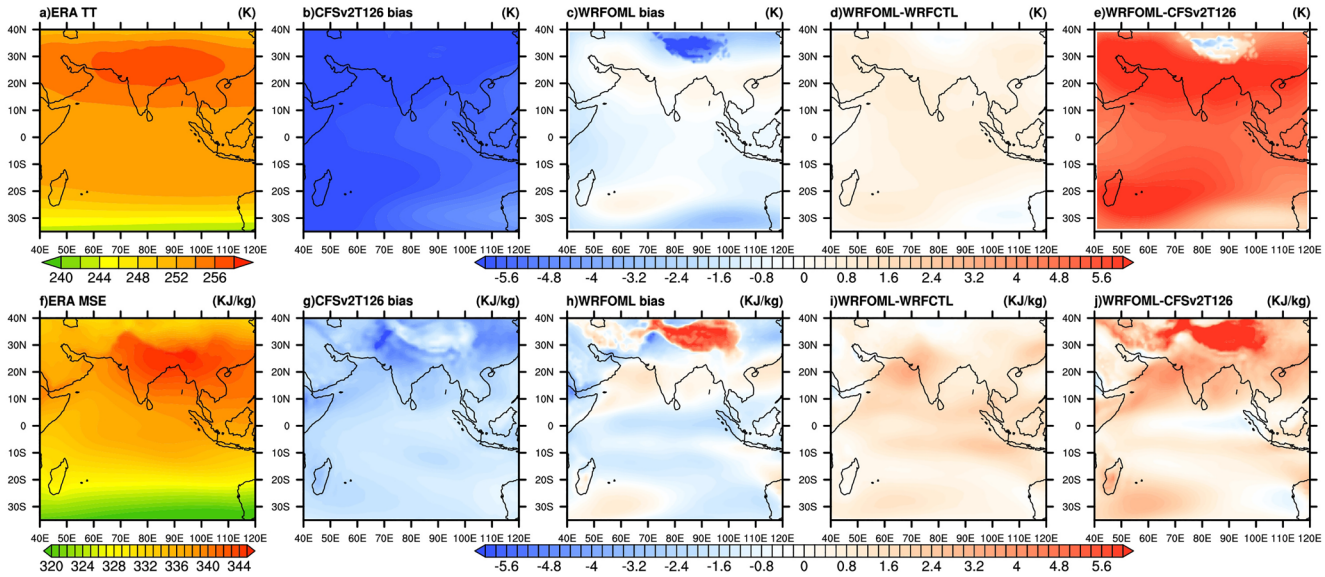

Figure 7. Spatial distribution of (a) mean tropospheric temperature (K) from observation, the biases from (b) CFSv2-T126 and (c) WRFOML and (d) difference between WRFOML and WRFCTL, (e) difference between WRFOML and CFSv2-T126. The lower panel (f–j) is the same as the upper panel but for MSE (KJ/kg).

The meridional phase speed of the northward propagating monsoon intraseasonal oscillation (MISOs) is directly proportional to the easterly vertical wind shear (Ajayamohan et al., 2008; Jiang et al., 2004). The difference between the zonal wind at 850 hPa and 200 hPa from observation and the respective biases of the two model simulations are shown in Figure 8. The simulated wind shear is stronger in WRFOML than in CFSv2-T126 and WRFCTL, indicating better simulation of MISOs (Sharmila et al., 2013). To investigate the source of the moisture for the initiation of the convection and the associated rainfall, vertically integrated (from the surface to 300 hPa) moisture in the JJAS season is calculated from the observation and models (Figures 8f–8j; bottom panel). Observation shows that a large amount of moisture is transporting from the southern Indian ocean, AS, and BoB to the Indian land region (Figure 8f). CFSv2-T126 shows substantial anomalous moisture divergence over the central Indian region and strong easterly bias over BoB, AS, and southern Indian regions (Figure 8g), enhancing dry bias over India. Coupled WRFOML simulated more

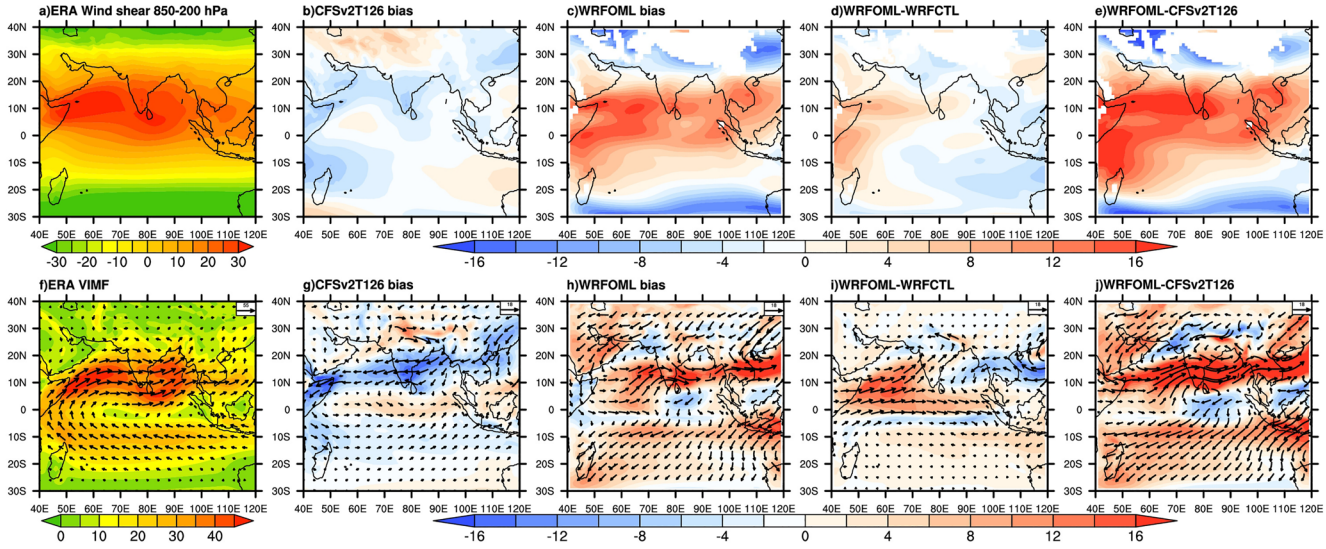

Figure 8. Spatial distribution of (a) mean zonal wind shear (m/s, 850−200 hPa) from observation, the biases from (b) CFSv2-T126 and (c) WRFOML and (d) difference between WRFOML and WRFCTL (e) difference between WRFOML and CFSv2-T126. The lower panel (f–j) is the same as the upper panel but for VIMF (KJ/kg).

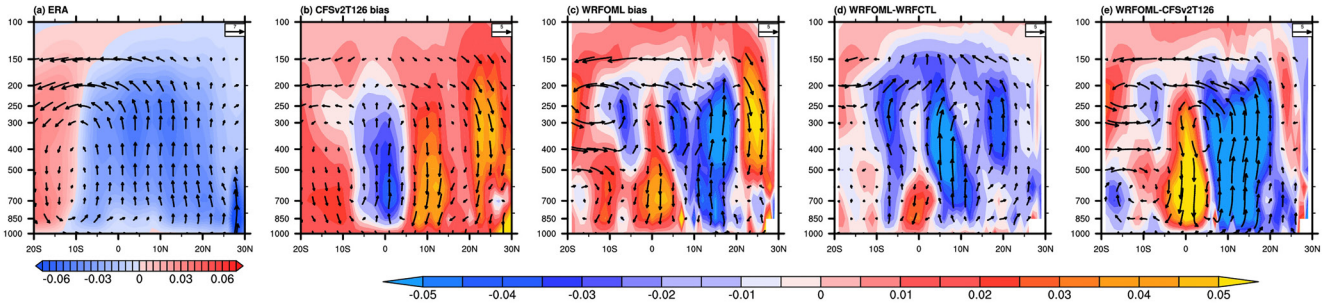

Figure 9. Latitude-pressure cross-section of (a) mean Hadley circulation averaged over 70–90°E, the biases from the models (b) CFSv2-T126 and (c) WRFOML and (d) the differences between WRFOML and WRFCTL, (e) difference between WRFOML and CFSv2-T126. The shades denote vertical velocity (Pa/s). The positive values indicate downward motion, and negative values indicate upward motion.

vertically integrated moisture over AS and equatorial Indian ocean region than the WRFCTL, which leads to improved precipitation over the central Indian region and south of the equator (0–10°S) (Figure 8h). Hence, WRFOML reasonably well simulated the vertically integrated moisture transport over central India compared to the CFSv2-T126 and WRFCTL, which leads to improved seasonal precipitation over the Indian region.

Earlier studies have linked the wet bias over the Equatorial Indian Ocean and dry bias over the Indian landmass may be a consequence of each other, likely related by the local Hadley cell (HC) noted by Slingo and Annamalai (2000) and B. B. Goswami et al. (2014). Figure 9 illustrates the JJAS mean local HC averaged over 70°–90°E from the observation and model biases. In observation, a steady ascending (negative vertical velocities) motion is observed over the Indian subcontinent (from 5°N to 20°N) and south of the equator (from the equator to 10°S), and stable descending (positive vertical velocities) motion is observed over latitudes around 10°S–20°S (Figure 9a). CFSv2-T126 simulates anomalous biases in ascending motion over the Indian Ocean and weak descending motion over the Indian landmass. These anomalous biases in ascending (descending) motion lead to the wet (dry) bias over the equatorial Indian Ocean (Indian landmass) region, and these results are consistent with the previous studies (Devanand et al., 2018; B. B. Goswami et al., 2014). WRFCTL simulated a weaker ascending motion over the equator to 10°S and over the Indian land region compared to WRFOML (Figure 9d), which leads to the increased dry bias over the ITCZ region and over the Indian landmass. The air-sea coupling in WRFOML improves the ascending motion over Indian latitudes and better simulated the HC with slight overestimation compared to the observation. The preceding discussion suggests that the WRFOML simulates the seasonal mean monsoon features better than the CFSv2-T126 and WRFCTL. The better JJAS mean rainfall can be attributed to the warm SST bias in the Indian Ocean and the improved TT gradient, which causes a more robust mean monsoon circulation. The more vigorous low-level circulation associated with warmer SSTs brings in lots of moisture from the ocean to the landmass, associated with a strong ascending branch of HC over northern latitudes, which produces more rainfall over India.

To study further the causes of improved JJAS mean features, biases of the vertical structure of dynamic and thermodynamic parameters over different regions, and climatological mean evolution of TT, specific humidity, vertical velocity, and MSE averaged over 70°–90°E are explored in the following section.

5. Mean Biases in Vertical Structures of Dynamic and Thermodynamic Parameters

5.1. Vertical Structures of Dynamic and Thermodynamic Parameters

In this section, we explore the vertical structures of temperature, specific humidity (q), MSE, and vertical velocity over Indian landmass and three convectively active regions (BoB, AS, and EqIO) in terms of biases in Figure 10. Both CFSv2-T126 and WRFCTL simulated a large cold bias (−1 to −3.8 K) from the middle to upper troposphere over the Indian landmass, BoB, and AS, which is significantly reduced in WRFOML (Figures 10a, 10e and 10i). The WRFOML shows a slight warm (cold) bias over BoB and AS (EqIO), which

10.1029/2020EA001507

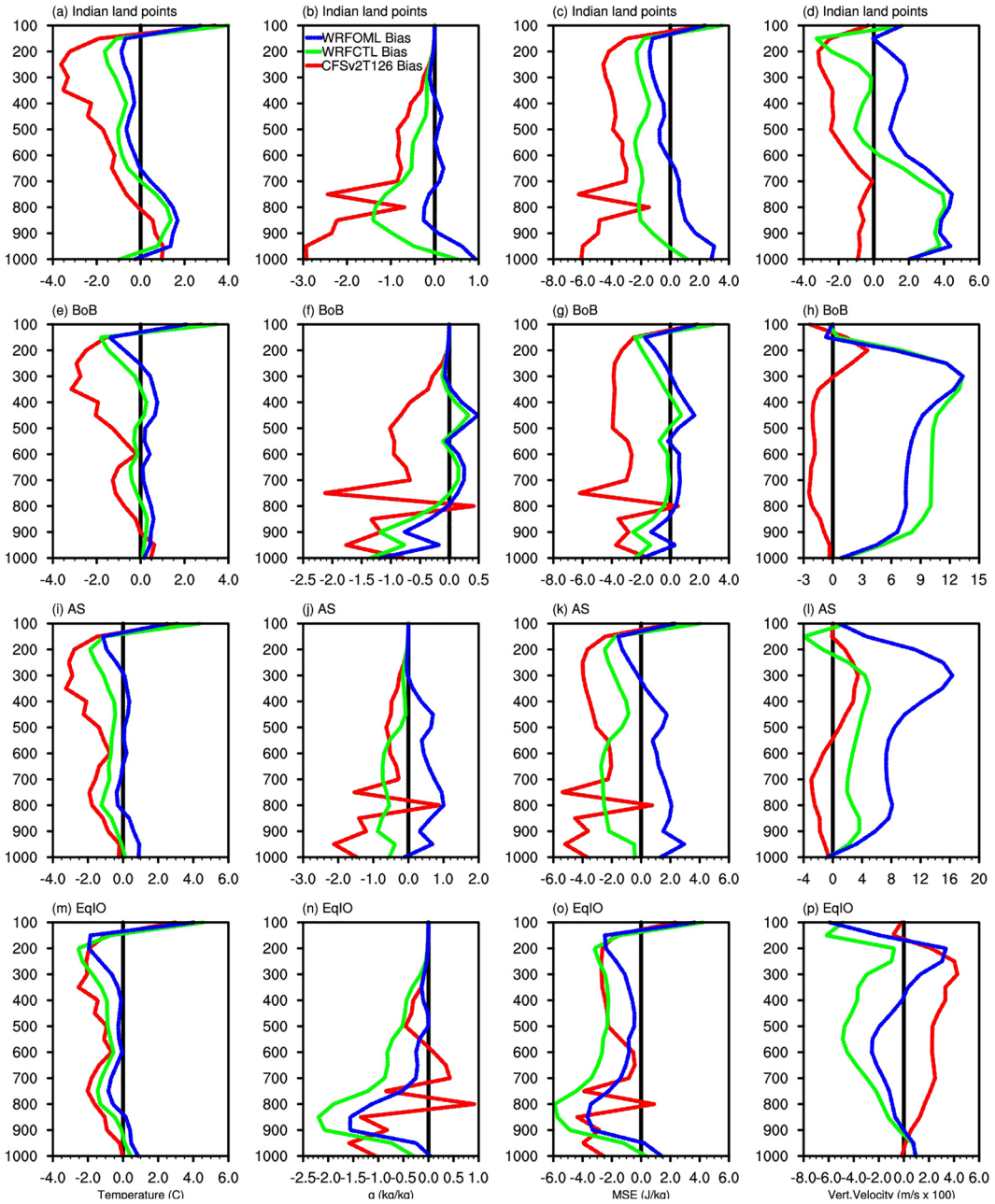

Figure 10. JJAS mean vertical biases of (a, e, i, m) tropospheric temperature (°C), (b, f, j, n) specific humidity (kg/kg), (c, g, k, o), moist static energy (J/kg), and (d, h, l, p) vertical velocity (*100 m/s). Red line represents CFSv2-T126, blue line for WRFOML and green line for WRFCTL.

can be attributed to the overestimation (underestimation) of latent heating associated with the wet (dry) bias (Figure 1f) over these regions. The vertical structure of specific humidity shows that the atmosphere in CFSv2-T126 and WRFCTL is relatively dry; it is not surprising, as the dry bias in these simulations is a direct outcome of this relatively dry atmosphere. WRFOML has more humidity in the troposphere over AS and BoB compared to CFSv2-T126 and WRFCTL. The availability of moisture is a precursor to stronger rainfall events in WRFOML (Figures 10b, 10f, 10j and 10n). The vertical profiles of MSE associated with ISM reveal that the CFSv2-T126 and WRFCTL simulations underestimate the MSE from lower to upper troposphere, indicating that the troposphere is less unstable over the Indian landmass, BoB, AS, and EqIO. In contrast, these biases are considerably reduced in WRFOML, which leads to the pumping of more moisture from

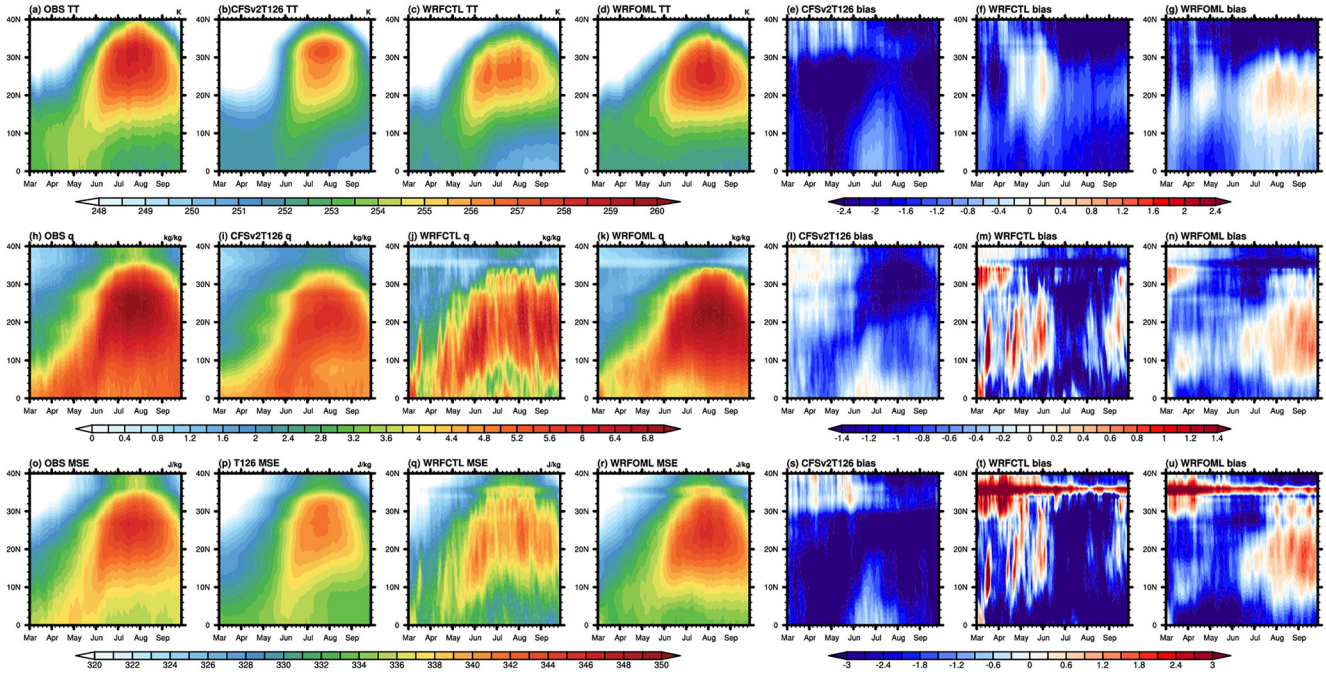

Figure 11. The time-latitude evolution of tropospheric temperature (K) (upper panel: a–g), specific humidity (kg/kg) (middle panel: h–n), and MSE (J/kg) (lower panel: o–u) averaged over the longitudes 70°–90°E. The first column (a, h, o) is observation, the second (CFSv2-T126: b, i, p), third column (WRFCTL: c, j, q), and fourth column (WRFOML: d, k, r) are from model simulations and fifth (CFSv2-T126: e, l, s), sixth (WRFCTL: f, m, t), and seventh (WRFOML: g, n, u) column show model biases from observation.

the lower to upper layers and results in wet precipitation bias (Figures 10g, 10k and 10o). CFSv2-T126 underestimates the vertical velocities over the Indian region, which leads to dry biases (Figure 10d). Both the regional model experiments significantly overestimate the vertical velocities over the Indian region, BoB, and AS, which indicates an abundance of convection. This enhanced mean ascent coupled with an unstable atmosphere and ample moisture availability cause reduced (enhanced) precipitation bias over India (BoB and AS; Figure 1e).

5.2. Time-Latitude Evolution of TT, Specific Humidity (q), and MSE Over Indian Longitudes

Figure 11 depicts the mean annual evolution of TT, q, and MSE averaged over 70°E and 90°E from models and observation. Observation shows a strong meridional gradient in climatological mean tropospheric temperature, more moist and anomalous MSE (unstable) after mid-May over Indian latitudes, which is consistent with a previous study by Xavier et al., 2007 (Figures 11a, 11h and 11o). As monsoon progresses northward, the associated convective heating, moist instability also moves to the north and reaches upto 34°N. WRFOML (Figures 11d, 11k and 11r) is able to reproduce the climatological JJAS mean TT, q, and MSE as in observation compared to WRFCTL (Figures 11c, 11j and 11q) and CFSv2-T126 (Figures 11b, 11i and 11p). CFSv2-T126 simulates strong cold biases (Figure 11e), dry biases in specific humidity (Figure 11l), and weakly unstable troposphere (Figure 11s). WRFCTL simulated a warm, wet and unstable troposphere from March to May; after the monsoon onset, it has a cold, dry, and weakly unstable troposphere (Figures 11f, 11m and 11t). It is noticed that the aforementioned biases are significantly reduced in WRFOML (Figures 11g, 11n and 11u). CFSv2-T126 and WRFCTL simulated significant cold, dry, and large MSE biases during the monsoon season, which leads to the dry bias over the central Indian region (Figure 1e). WRFOML simulates warm, wet, and relatively more unstable troposphere, which reduces the dry bias over the central Indian region (Figure 1f). Thus, it indicates that the WRFOML simulates the realistic thermodynamic structure of the atmosphere during the JJAS season, leading to better simulation of large-scale Indian monsoon precipitation.

6. Summary

The seasonal prediction of ISMR using coupled global models has attained a reasonably good skill (Rao et al., 2019). Even though the country averaged forecasts are an essential metric for the socio-economic planners, there is an increasing demand for higher resolution model forecasts from an application perspective (e.g., agricultural or hydrological purposes). Running a CGCM at a finer resolution to meet the demands of hydrological or crop models is very expensive in terms of the computation cost. Therefore, this study aims to examine whether this gap between coarse resolution seasonal forecasts and application models can be bridged by employing dynamical downscaling. The role of air-sea interaction on the simulated ISM mean features is examined by an uncoupled WRF (WRFCTL) and a coupled WRF model (WRFOML) to dynamically downscale the CFSv2-T126 reforecasts for the period 1982–2017 using the February Initial conditions over the Indian Monsoon domain. CFSv2-T126 and WRFCTL suffer from a robust dry bias over Indian landmass, which stems from the cold SST bias over the Indian Ocean, weak meridional tropospheric temperature gradient, and strong anti-cyclonic circulation bias. Seasonal mean dry bias over the central Indian region is significantly reduced in WRFOML due to the warm SST bias in the Indian Ocean and realistic simulation of LLJ over AS, which supplies a large amount of moisture to the Indian land region. WRFOML could reproduce the ascending branch of HC over Indian latitudes as in observation compared to CFSv2-T126 and WRFCTL (Figure 9), which also contributed to the reduction in seasonal mean bias over the Indian region (Figure 1f). Weak TT gradient causes a delayed monsoon onset over India in CFSv2-T126, whereas WRFOML realistically simulated TT gradient, which leads to a realistic simulation of monsoon onset. The timing and seasonal mean biases in different dynamic and thermodynamic parameters of monsoon improved significantly in the downscaled WRFOML simulation compared to CFSv2-T126 and WRFCTL. All these improvements result in a dramatic reduction in dry bias over the Indian landmass. The improvements are not only limited to the seasonal mean rainfall but also the simulation of the number of rainy days improved over the country as a whole and the different homogenous regions of the Indian monsoon. A long-standing problem in the CFSv2-T126 is that it over-estimates the light rainfall events and significantly under-estimates the contributions from moderate and heavy rainfall events (Krishna et al., 2019). Owing to the better representation of small-scale processes in the higher resolution downscaled simulations, the mean and distribution of light, moderate, and heavy rain category events have improved significantly in WRFOML though the seasonal mean skill has remained almost the same as CFSv2-T126. WRFCTL and CFSv2-T126 simulations unable to capture the correct phase of ISMR in many years compared to WRFOML. It is noticed that a considerable reduction in the dry bias over the Indian region in WRFOML (16%) compared to CFSv2-T126 (44%) and WRFCTL (33%). The overall improvements reported here have substantial implications for various socio-economic sectors in India, such as agriculture and hydrology. The crop models are basically rainfall-driven. The improvements in the simulation of different rain rate categories are expected to translate to the sectoral application-based forecasts derived from the downscaled simulations. Even though the mean monsoon precipitation significantly improved in WRFOML compared to WRFCTL and CFSv2-T126, still further improvement in the precipitation is required. WRFOML lacks full ocean dynamics, which is one of the limitations of this model to address all aspects of ISMR. These will be attempted and reported elsewhere. Further improvements to the CGCM and resolution enhancements to WRFOML are expected to deliver promising results and are yet to be explored.

Data Availability Statement

Monthly observed Optimum Interpolated SST is available from https://psl.noaa.gov/data/gridded/data.noaa.oisst.v2.html (OISST, Reynolds et al., 2002). Rainfall product from Global Precipitation Climatology Project is available from https://rda.ucar.edu/datasets/ds728.3/ (GPCP, Adler et al., 2003); daily gridded rainfall data from India Meteorological Department is available at http://www.imdpune.gov.in/Clim_Pred_LRF_New/Grided_Data_Download.html at 1° × 1 ° resolution (Rajeevan et al., 2006), and Tropical Rainfall Measuring Mission (TRMM) estimated monthly precipitation is available from https://disc.gsfc.nasa.gov/datasets/TRMM_3B42_Daily_7/summary (3B43V7, Huffman et al., 2007). European Center for Medium Weather Forecast (ECMWF) interim reanalysis (ERA-interim, Dee et al., 2011) monthly data products such as winds, air temperature, specific humidity at different levels, sea level pressure (SLP) are available from https://apps.ecmwf.int/datasets/data/interim-full-daily/levtype=pl/. MLD data used to initialize the Ocean

model is obtained from https://www.metoffice.gov.uk/hadobs/en4/, which is based on observed Ocean temperature and salinity profiles.

Acknowledgments
Indian Institute of Tropical Meteorology (IITM) is fully funded by the Ministry of Earth Sciences. The authors are grateful to NCAR, Boulder, Colorado, USA, for making the WRF-ARW model available. We also thank ECMWF (http://apps.ecmwf.int/datasets/data/interim_full_daily/) for providing the reanalysis data sets. Data used to generate plots in the paper are available in the following public domain repository: https://ardc.tropmet.res.in/thredds/esspaper.html. We thank the NCAR for making available the NCAR Command Language (NCL). All data sources are duly acknowledged. The authors are very grateful to the editor and the anonymous reviewers for providing valuable suggestions and comments.

References

Abhik, S., Mukhopadhyay, P., & Goswami, B. N. (2013). Evaluation of mean and intraseasonal variability of Indian summer monsoon simulation in ECHAM5: Identification of possible source of bias. *Climate Dynamics*, *43*, 389–406. https://doi.org/10.1007/s00382-013-1824-7

Adler, R. F., Huffman, G. J., Chang, A., Ferraro, R., Xie, P. P., Janowiak, J., et al. (2003). The version-2 Global Precipitation Climatology Project (GPCP) monthly precipitation analysis (1979–present). *Journal of Hydrometeorology*, *4*, 1147–1167. https://doi.org/10.1175/1525-7541(2003)004<1147:TVGPCP>2.0.CO;2

Ajayamohan, R. S., Rao, S. A., & Yamagata, T. (2008). Influence of Indian Ocean dipole on poleward propagation of boreal summer intraseasonal oscillations. *Journal of Climate*, *21*, 5437–5454. https://doi.org/10.1175/2008jcli1758.1

Betts, A. K., & Miller, M. J. (1986). A new convective adjustment scheme. Part II: Single column tests using GATE wave, BOMEX, ATEX and arctic air-mass data sets. *Quarterly Journal of Royal Meteorological Society*, *112*, 693–709. https://doi.org/10.1002/qj.49711247308

Bhaskar Rao, D. V., Ashok, K., & Yamagata, T. (2004). A numerical simulation study of the Indian summer monsoon of 1994 using NCAR MM5. *Journal of the Meteorological Society of Japan*, *82*(6), 1755–1775. https://doi.org/10.2151/jmsj.82.1755

Bhaskaran, B., Jones, R. G., Murphy, J. M., & Noguer, M. (1996). Simulation of the Indian summer monsoon using a nested regional climate model: Domain size experiments. *Climate Dynamics*, *12*, 573–587. https://doi.org/10.1007/bf00216267

Capa-Morocho, M., Ines, A. V. M., Baethgen, W. E., Rodriguez-Fonseca, B., Han, E., & Ruiz-Ramos, M. (2016). Crop yield outlooks in the Iberian Peninsula: Connecting seasonal climate forecasts with crop simulation models. *Agricultural Systems*, *149*, 75–87. https://doi.org/10.1016/j.agsy.2016.08.008

Chen, F., Pielke, R. A., & Mitchell, K. (2001). Development and application of land-surface models for mesoscale atmospheric models: Problems and promises. In V. Lakshmi, J. Albertson, & J. Schaake (Eds.), *Land surface hydrology, meteorology, and climate: Observations and modeling of water science and application* (Vol. 3, pp. 107–135). Washington: American Geophysical Union. https://doi.org/10.1029/ws003p0107

Chen, X., Pauluis, O. M., & Zhang, F. (2018). Regional simulation of Indian summer monsoon intraseasonal oscillations at gray-zone resolution. *Atmospheric Chemistry and Physics*, *18*(2), 1003–1022. https://doi.org/10.5194/acp-18-1003-2018

Dai, A. (2006). Precipitation characteristics in eighteen coupled climate models. *Journal of Climate*, *19*, 4605–4630. https://doi.org/10.1175/JCLI3884.1

Dash, S. K., Pattnayak, K. C., Panda, S. K., Vaddi, D., & Mamgain, A. (2014). Impact of domain size on the simulation of Indian summer monsoon in RegCM4 using mixed convection scheme and driven by HadGEM2: Impact of domain size on ISM simulations. *Climate Dynamics*, *44*, 961–975. https://doi.org/10.1007/s00382-014-2420-1

Davis, C., Wang, W., Chen, S. S., Chen, Y., Corbosiero, K., Demaria, M., et al. (2008). Prediction of landfalling hurricanes with the advanced hurricane WRF model. *Monthly Weather Review*, *136*, 1990–2005. https://doi.org/10.1175/2007MWR2085.1

Dee, D. P., Uppala, S. M., Simmons, A. J., Berrisford, P., Poli, P. P., Kobayashi, S., et al. (2011). The ERA-interim reanalysis: Configuration and performance of the data assimilation system. *Quarterly Journal of the Royal Meteorological Society*, *137*, 553–597. https://doi.org/10.1002/qj.828

Devanand, A., Roxy, M. K., & Ghosh, S. (2018). Coupled land-atmosphere regional model reduces dry bias in Indian summer monsoon rainfall simulated by CFSv2. *Geophysical Research Letters*, *45*, 2476–2486. https://doi.org/10.1002/2018GL077218

Di Luca, A., de Elía, R., & Laprise, R. (2012). Potential for added value in precipitation simulated by high-resolution nested regional climate models and observations. *Climate Dynamics*, *38*, 1229–1247. https://doi.org/10.1007/s00382-011-1068-3

Dobler, A., & Ahrens, B. (2010). Analysis of the Indian summer monsoon system in the regional climate model COSMO-CLM. *Journal of Geophysical Research*, *115*, D16101. https://doi.org/10.1029/2009JD013497

Ek, M. B., Mitchell, K. E., Lin, Y., Rogers, E., Grunmann, P., Koren, V., et al. (2003). Implementation of Noah land surface model advances in the national centers for environmental prediction operational mesoscale Eta model. *Journal of Geophysical Research*, *108*, 2002JD003296. https://doi.org/10.1029/2002JD003296

Emanuel, K. A., Neelin, J. D., & Bretherton, C. S. (1994). On large-scale circulations in convecting atmospheres. *Quarterly Journal of Royal Meteorological Society*, *120*, 1111–1143. https://doi.org/10.1002/qj.49712051902

Fasullo, J., & Webster, P. J. (2003). A hydrological definition of Indian monsoon onset and withdrawal. *Journal of Climate*, *16*, 3200–3211. https://doi.org/10.1175/1520-0442(2003)016<3200a:AHDOIM>2.0.CO;2

Findlater, J. (1969). A major low-level air current near the Indian Ocean during the northern summer. *Quarterly Journal of Royal Meteorological Society*, *95*, 362–380. https://doi.org/10.1002/qj.49709540409

Gadgil, S., & Gadgil, S. (2006). The Indian monsoon, GDP and agriculture. *Economic and Political Weekly*, *41*, 4887–4895. https://doi.org/10.2307/4418949

George, G., Rao, D. N., Sabeerali, C. T., Ankur, S., & Suryachandra, A. R. (2016). Indian summer monsoon prediction and simulation in CFSv2 coupled model. *Atmospheric Science Letters*, *17*, 57–64. https://doi.org/10.1002/asl.599

Giorgi, F., & Gutowski, Jr, W. J. (2015). Regional dynamical downscaling and the CORDEX initiative. *Annual Review of Environmental Resources*, *40*, 467–490. https://doi.org/10.1146/annurev-environ-102014-021217

Goswami, B. B., Deshpande, M., Mukhopadhyay, P., Saha, S. K., Rao, S. A., Raghu, M., & Goswami, B. N. (2014). Simulation of monsoon intraseasonal variability in NCEP CFSv2 and its role on systematic bias. *Climate Dynamics*, *43*, 2725–2745. https://doi.org/10.1007/s00382-014-2089-5

Goswami, B. N., & Xavier, P. K. (2005). ENSO control on the south Asian monsoon through the length of the rainy season. *Geophysical Research Letters*, *32*, 1–n. https://doi.org/10.1029/2005GL023216

Griffies, S. M., Harrison, M. J., Pacanowski, R. C., & Rosati, A. (2004). *A technical guide to MOM4, GFDL ocean group technical report no. 5*. NOAA/Geophysical Fluid Dyn Lab. Retrieved from www.gfdl.noaa.gov

Hari Prasad, D., Srinivas, C. V., Bhaskar Rao, D. V., & Anjaneyulu, Y. (2011). Simulation of Indian monsoon extreme rainfall events during the decadal period 2000–2009 using a high resolution mesoscale model. *Advances in Geosciences*, *A6*, 31–48.

Huffman, G. J., Adler, R. F., Bolvin, D. T., Gu, G., Nelkin, E. J., Bowman, K. P., et al. (2007). The TRMM multisatellite precipitation analysis (TMPA): Quasi-global, multiyear, combined-sensor precipitation estimates at fine scales. *Journal of Hydrometeorology*, *8*, 38–55. https://doi.org/10.1175/JHM560.1

Iacono, M. J., Delamere, J. S., Mlawer, E. J., Shephard, M. W., Clough, S. A., & Collins, W. D. (2008). Radiative forcing by long-lived greenhouse gases: Calculations with the AER radiative transfer models. *Journal of Geophysical Research*, *113*, D13103. https://doi.org/10.1029/2008JD009944

Jacob, D., & Podzun, R. (1997). Sensitivity studies with the regional climate model REMO. *Meteorology Atmosphere and Physics*, *63*, 119–129. https://doi.org/10.1007/BF01025368

Janjic, Z. I. (1994). The step-mountain Eta coordinate model: Further developments of the convection, viscous sublayer, and turbulence closure schemes. *Monthly Weather Review*, *122*, 927–945. https://doi.org/10.1175/1520-0493(1994)122<0927:TSMECM>2.0.CO;2

Janjic, Z. I. (2000). Comments on "development and evaluation of a convection scheme for use in climate models". *Journal of Atmospheric Science*, *57*, 3686.

Jiang, X., Li, T., & Wang, B. (2004). Structures and mechanisms of the northward propagating boreal summer intraseasonal oscillation. *Journal of Climate*, *17*, 1022–1039. https://doi.org/10.1175/1520-0442(2004)017<1022:samotn>2.0.co;2

Joseph, P. V., & Raman, P. L. (1966). Existence of low level westerly jet-stream over peninsular India during July. *Indian Journal of Meteorology, Hydrology and Geophysics*, *17*, 407–410.

Juang, H. M. H., Hong, S. Y., & Kanamitsu, M. (1997). The NCEP regional spectral model: An update. *Bulletin of the American Meteorological Society*, *78*, 2125–2143. https://doi.org/10.1175/1520-0477(1997)078<2125:TNRSMA>2.0.CO;2

Kim, D., Kug, J. S., & Sobel, A. H. (2014). Propagating versus nonpropagating Madden-Julian oscillation events. *Journal of Climate*, *27*, 111–125. https://doi.org/10.1175/JCLI-D-13-00084.1

Konduru, R. T., & Takahashi, H. G. (2020). Effects of convection representation and model resolution on diurnal precipitation cycle over the Indian monsoon region: Toward a convection-permitting regional climate simulation. *Journal of Geophysical Research: Atmospheres*, *125*. https://doi.org/10.1029/2019JD032150

Krishna, R. P. M., Rao, S. A., Srivastava, A., Hari Prasad, K., Maheswar, P., Prasanth, P., et al. (2019). Impact of convective parameterization on the seasonal prediction skill of Indian summer monsoon. *Climate Dynamics*, *53*, 1–6243. https://doi.org/10.1007/s00382-019-04921-y

Lee, D. K., & Suh, M. S. (2000). Ten year East Asian summer monsoon simulation using a regional climate model (RegCM2). *Journal of Geophysical Research*, *105*, 29565–29577. https://doi.org/10.1029/2000jd900438

Lim, K. S. S., & Hong, S. Y. (2010). Development of an effective double-moment cloud microphysics scheme with prognostic cloud condensation nuclei (CCN) for weather and climate models. *Monthly Weather Review*, *138*, 1587–1612. https://doi.org/10.1175/2009MWR2968.1

Lucas-Picher, P., Christensen, J. H., Saeed, F., Kumar, P., Ahrens, B., Wiltshire, A. J., et al. (2011). Can regional climate models represent the Indian monsoon? *Journal of Hydrometeorology*, *12*, 849–868. https://doi.org/10.1175/2011jhm1327.1

Maharana, P., & Dimri, A. P. (2016). Study of intraseasonal variability of Indian summer monsoon using a regional climate model. *Climate Dynamics*, *46*, 1043–1064. https://doi.org/10.1007/s00382-015-2631-0

Manzanas, R., Gutiérrez, J. M., Fernández, J., Meijgaard, E. V., Calmanti, S., Magarino, M. E., et al. (2018). Dynamical and statistical downscaling of seasonal temperature forecasts in Europe: Added value for user applications. *Climate Service*, *9*, 44–56. https://doi.org/10.1016/j.cliser.2017.06.004

Mellor, G. L., & Yamada, T. (1982). Development of a turbulence closure model for geophysical fluid problems. *Reviews of Geophysics*, *20*, 851. https://doi.org/10.1029/RG020i004p00851

Misra, V., Mishra, A., & Bhardwaj, A. (2018). Simulation of the intraseasonal variations of the Indian summer monsoon in a regional coupled ocean-atmosphere model. *Journal of Climate*, *31*(8), 3167–3185. https://doi.org/10.1175/JCLI-D-17-0434.1

Mukhopadhyay, P., Taraphdar, S., Goswami, B. N., & Krishnakumar, K. (2010). Indian summer monsoon precipitation climatology in a high-resolution regional climate model: Impacts of convective parameterization on systematic biases. *Weather and Forecasting*, *25*, 369–387. https://doi.org/10.1175/2009WAF2222320.1

Pai, D. S., SuryachandraRao, A., Senroy, S., Maheswar, P., Prasanth, A. P., & Rajeevan, M. (2017). Performance of the operational and experimental long-range forecasts for the 2015 southwest monsoon rainfall. *Current Science*, *112*, 68–75. https://doi.org/10.18520/cs/v112/i01/68-75

Pillai, P. A., Rao, S. A., Ramu, D. A., Pradhan, M., & George, G. (2018). Seasonal prediction skill of Indian summer monsoon rainfall in NMME models and monsoon mission CFSv2. *International Journal of Climatology*, *38*, e847–e861. https://doi.org/10.1002/joc.5413

Pokhrel, S., Dhakate, A., Chaudhari, H. S., & Saha, S. K. (2013). Status of NCEP CFS vis-a-vis IPCC AR4 models for the simulation of Indian summer monsoon. *Theoretical and Applied Climatology*, *111*, 65–78. https://doi.org/10.1007/s00704-012-0652-8

Pollard, R. T., Rhines, P. B., & Thompson, R. O. R. Y. (1972). The deepening of the wind-mixed layer. *Geophysical Fluid Dynamics*, *4*, 381–404. https://doi.org/10.1080/03091927208236105

Pradhan, M., Rao, A. S., Srivastava, A., Dakate, A., Salunke, K., & Shameera, K. S. (2017). Prediction of Indian summer-monsoon onset variability: A season in advance. *Scientific Reports*, *7*, 1–14. https://doi.org/10.1038/s41598-017-12594-y

Rajeevan, M., Bhate, J., Kale, J. D., & Lal, B. (2006). High resolution daily gridded rainfall data for the Indian region: Analysis of break and active monsoon spells. *Current Science*, *91*(3), 296–306.

Rajeevan, M., Rohini, P., Niranjan Kumar, K., Srinivasan, J., & Unnikrishnan, C. K. (2013). A study of vertical cloud structure of the Indian summer monsoon using CloudSat data. *Climate Dynamics*, *40*, 637–650. https://doi.org/10.1007/s00382-012-1374-4

Raju, A., Parekh, A., Chowdary, J. S., & Gnanaseelan, C. (2015). Assessment of the Indian summer monsoon in the WRF regional climate model. *Climate Dynamics*, *44*, 3077–3100. https://doi.org/10.1007/s00382-014-2295-1

Raju, A., Parekh, A., Chowdary, J. S., & Gnanseelan, C. (2014). Impact of satellite retrieved atmospheric temperature profiles assimilation on Asian summer monsoon simulation. *Theoretical and Applied Climatology*, *116*, 317–326. https://doi.org/10.1007/s00704-013-0956-3

Raju, A., Parekh, A., & Gnanaseelan, C. (2014). Evolution of vertical moist thermodynamic structure associated with the Indian summer monsoon in a regional climate model. *Pure and Applied Geophysics*, *171*(7), 1499–1518. https://doi.org/10.1007/s00024-013-0697-3

Ramu, D. A., Rao, S. A., Pillai, P. A., Pradhan, M., George, G., Nagarjuna Rao, D., et al. (2017). Prediction of seasonal summer monsoon rainfall over homogenous regions of India using dynamical prediction system. *Journal of Hydrology*, *546*, 103–112. https://doi.org/10.1016/j.jhydrol.2017.01.010

Ramu, D. A., Sabeerali, C. T., Chattopadhyay, R., Nagarjuna Rao, D., Gibies, G., Dhakate, A. R., et al. (2016). Indian summer monsoon rainfall simulation and prediction skill in the CFSv2 coupled model: Impact of atmospheric horizontal resolution. *Journal of Geophysical Research: Atmosphere*, *121*, 2205–2221. https://doi.org/10.1002/2015JD024629

Rao, S. A., Goswami, B. N., Sahai, A. K., Rajagopal, E. N., Mukhopadhyay, P., Rajeevan, M., et al. (2019). Monsoon mission: A targeted activity to improve monsoon prediction across scales. *Bulletin of American Meteorological Society*, *100*, 2509–2532. https://doi.org/10.1175/BAMS-D-17-0330.1

Ratnam, J. V., Behera, S. K., Ratna, S. B., Rautenbach, C. J. de W., Lennard, C., Luo, J. J., et al. (2013). Dynamical downscaling of austral summer climate forecasts over Southern Africa using a regional coupled model. *Journal of Climate*, *26*, 6015–6032. https://doi.org/10.1175/JCLI-D-12-00645.1

Reynolds, R. W., Rayner, N. A., Smith, T. M., Stokes, D. C., & Wang, W. (2002). An improved in situ and satellite SST analysis for climate. *Journal of Climate*, *15*, 1609–1625. https://doi.org/10.1175/1520-0442(2002)015<1609:aiisas>2.0.co;2

Sabeerali, C. T., Ramu, D. A., Dhakate, A., Salunke, K., Mahapatra, S., & Rao, S. A. (2013). Simulation of boreal summer intraseasonal oscillations in the latest CMIP5 coupled GCMs. *Journal of Geophysical Research: Atmosphere*, *118*, 4401–4420. https://doi.org/10.1002/jgrd.50403

Sabin, T. P., Krishnan, R., Ghattas, J., Denvil, S., Dufresne, J. L., Hourdin, F., & Pascal, T. (2013). High resolution simulation of the South Asian monsoon using a variable resolution global climate model. *Climate Dynamics*, *41*, 173–194. https://doi.org/10.1007/s00382-012-1658-8

Saeed, F., Hagemann, S., & Jacob, D. (2012). A framework for the evaluation of the South Asian summer monsoon in a regional climate model applied to REMO. *International Journal of Climatology*, *32*, 430–440. https://doi.org/10.1002/joc.2285

Saha, S., Moorthi, S., Wu, X., Wang, J., Nadiga, S., Tripp, P., et al. (2014). The NCEP climate forecast system version 2. *Journal of Climate*, *27*, 2185–2208. https://doi.org/10.1175/JCLI-D-12-00823.1

Saha, S. K., Pokhrel, S., Chaudhari, H. S., Dhakate, A., Shewale, S., Sabeerali, C. T., et al. (2013). Improved simulation of Indian summer monsoon in latest NCEP climate forecast system free run. *International Journal of Climatology*, *34*, 1628–1641. https://doi.org/10.1002/joc.3791

Saha, S. K., Pokhrel, S., Salunke, K., Dhakate, A., Chaudhari, H. S., Rahaman, H., et al. (2016). Potential predictability of Indian summer monsoon rainfall in NCEP CFSv2. *Journal of Advances in Model Earth Systems*, *8*, 96–120. https://doi.org/10.1002/2015MS000542

Samanta, D., Hameed, S. N., Jin, D., Thilakan, V., Ganai, M., Rao, S. A., & Deshpande, M. (2018). Impact of a narrow coastal Bay of Bengal sea surface temperature front on an Indian summer monsoon simulation. *Scientific Reports*, *8*, 1–12. https://doi.org/10.1038/s41598-018-35735-3

Sharmila, S., Pillai, P. A., Joseph, S., Roxy, M., Krishna, R. P. M., Chattopadhyay, R., et al. (2013). Role of ocean–atmosphere interaction on northward propagation of Indian summer monsoon intra-seasonal oscillations (MISO). *Climate Dynamics*, *41*, 1651–1669. https://doi.org/10.1007/s00382-013-1854-1

Skamarock, W. C., Klemp, J. B., Dudhia, J., Gill, D. O., Barker, D. M., Duda, M. G., et al. (2008). *A description of the advanced research WRF Version 3. NCAR Technical Note, NCAR/TN-475+STR*. Boulder: Mesoscale and Microscale Meteorology Division, National Center for Atmospheric Research.

Slingo, J. M., & Annamalai, H. (2000). 1997: The El Niño of the century and the response of the Indian summer monsoon. *Monthly Weather Review*, *128*, 1778–1797. https://doi.org/10.1175/1520-0493(2000)128<1778:tenoot>2.0.co;2

Srinivas, C. V., Hari Prasad, D., Bhaskar Rao, D. V., Anjaneyulu, Y., Baskarana, R., & Venkataramana, B. (2012). Simulation of the Indian summer monsoon regional climate using advanced research WRF model. *International Journal of Climatology*, *33*, 1195–1210. https://doi.org/10.1002/joc.3505

Srinivas, C. V., Hariprasad, D., Rao, D. V. B., Anjaneyulu, Y., Baskaran, R., & Venkatraman, B. (2013) Simulation of the Indian summer monsoon regional climate using advanced research WRF model. *International Journal of Climatology*, *33*, 1195–1210. https://doi.org/10.1002/joc.3505

Srivastava, A., Rao, S. A., Rao, D. N., Gibies, G., & Maheswar, P. (2017). Structure, characteristics, and simulation of monsoon low-pressure systems in CFSv2 coupled model. *Journal of Geophysical Research: Ocean*, *122*, 6394–6415. https://doi.org/10.1002/2016JC012322

Stéfanon, M., Drobinski, P., D'Andrea, F., Brossier, C. L., & Bastin, S. (2014). Soil moisture-temperature feedbacks at meso-scale during summer heat waves over Western Europe. *Climate Dynamics*, *42*, 1309–1324. https://doi.org/10.1007/s00382-013-1794-9

Swathi, M. S., Izumo, T., Lengaigne, M., Vialard, J., & Ramesh Kumar, M. R. (2020). Remote influences on the Indian monsoon low-level jet intraseasonal variations. *Climate Dynamics*, *54*, 2221–2236. https://doi.org/10.1007/s00382-019-05108-1

Torma, C., Giorgi, F., & Coppola, E. (2015). Added value of regional climate modeling over areas characterized by complex terrain-precipitation over the Alps. *Journal of Geophysical Research*, *120*, 3957–3972. https://doi.org/10.1002/2014JD022781

Umakanth, U., Kesarkar, A. P., Raju, A., & VijayaBhaskar, R. S. (2016). Representation of monsoon intraseasonal oscillations in regional climate model: Sensitivity to convective physics. *Climate Dynamics*, *47*, 895–917. https://doi.org/10.1007/s00382-015-2878-5

Vellore, R. K., Krishnan, R., Pendharkar, J., Choudhury, A. D., & Sabin, T. P. (2014). On the anomalous precipitation enhancement over the Himalayan foothills during monsoon breaks. *Climate Dynamics*, *43*, 2009–2031. https://doi.org/10.1007/s00382-013-2024-1

Vernekar, A. D., & Ji, Y. (1999).Simulation of the onset and intraseasonal variability of two contrasting summer monsoons. *Journal of Climate*, *12*, 1707–1725. https://doi.org/10.1175/1520-0442(1999)012<1707:SOTOAI>2.0.CO;2

Wu, L., Wong, S., Wang, T., & Huffman, G. J. (2018). Moist convection: A key to tropical wave–moisture interaction in Indian monsoon intraseasonal oscillation. *Climate Dynamics*, *51*, 3673–3684. https://doi.org/10.1007/s00382-018-4103-9

Xavier, P. K., Marzin, C., & Goswami, B. N. (2007). An objective definition of the Indian summer monsoon season and a new perspective on the ENSO–monsoon relationship. *Quarterly Journal of the Royal Meteorological Society*, *133*, 749–764. https://doi.org/10.1002/qj.45

Xue, Y., Janjic, Z., Dudhia, J., Vasic, R., & Sales, F. D. (2014). A review on regional dynamical downscaling in intraseasonal to seasonal simulation/prediction and major factors that affect downscaling ability. *Atmospheric Research*, *147–148*, 68–85. https://doi.org/10.1016/j.atmosres.2014.05.001